Lamellar Diblock Copolymer Thin Films during Solvent Vapor Annealing Studied by GISAXS

Different Behavior of Parallel and Perpendicular Lamellae

Zhang, Jianqi; Posselt, Dorthe; Smilgies, Detlef-M.; Perlich, Jan; Kyriakos, Konstantinos; Jaksch, Sebastian ; Papadakis, Christine M.

Published in:
Macromolecules

DOI:
10.1021/ma500633b

Publication date:
2014

Document Version
Publisher's PDF, also known as Version of record

Citation for published version (APA):
Zhang, J., Posselt, D., Smilgies, D-M., Perlich, J., Kyriakos, K., Jaksch, S., & Papadakis, C. M. (2014). Lamellar Diblock Copolymer Thin Films during Solvent Vapor Annealing Studied by GISAXS: Different Behavior of Parallel and Perpendicular Lamellae. *Macromolecules*, *47*(16), 5711-5718. https://doi.org/10.1021/ma500633b

Macromolecules

ACS AuthorChoice

Article

pubs.acs.org/Macromolecules

Open Access on 08/15/2015

Lamellar Diblock Copolymer Thin Films during Solvent Vapor Annealing Studied by GISAXS: Different Behavior of Parallel and Perpendicular Lamellae

Jianqi Zhang,*[,†] Dorthe Posselt,[‡] Detlef-M. Smilgies,[§] Jan Perlich,[∥] Konstantinos Kyriakos,[†] Sebastian Jaksch,[†] and Christine M. Papadakis[†]

[†]Physik-Department, Fachgebiet Physik weicher Materie, Technische Universität München, James-Franck-Str. 1, 85748 Garching, Germany

[‡]IMFUFA, Department of Science, Systems and Models, Roskilde University, P.O. Box 260, 4000 Roskilde, Denmark

[§]Cornell High Energy Synchrotron Source (CHESS), Wilson Laboratory, Cornell University, Ithaca, New York 14853, United States

[∥]Deutsches Elektronen-Synchrotron (DESY), Notkestr. 85, 22607 Hamburg, Germany

Supporting Information

ABSTRACT: The reorientation of lamellae and the dependence of the lamellar spacing, D_{lam}, on polymer volume fraction, ϕ_P, $D_{lam} \propto \phi_P^{-\beta}$, in diblock copolymer thin films during solvent vapor annealing (SVA) are examined by combining white light interferometry (WLI) and grazing-incidence small-angle X-ray scattering (GISAXS). A thin film of lamellae-forming poly(styrene-*b*-butadiene) prepared by spin-coating features lamellae of different orientations with the lamellar spacing depending on orientation. During annealing with ethyl acetate (EAC) vapor, it is found that perpendicular lamellae behave differently from parallel ones, which is due to the fact that their initial lamellar thicknesses differ strongly. Quantitatively, the swelling process is composed of three regimes and the drying process of two regimes. The first two regimes of swelling are associated with a significant structural rearrangement of the lamellae; i.e., the lamellae first become thicker, and then perpendicular and randomly oriented lamellae vanish, which results in a purely parallel orientation at the end of the swelling process. The rearrangement is attributed to the increase of mobility of the polymer chains imparted by the solvent and to a decrease of total free energy of the thin film. In the third regime of swelling, the scaling exponent is found to be $\beta = -0.32$. During drying, the deswelling is nonaffine which may be a consequence of the increase of nonfavorable segmental interactions as the solvent is removed.

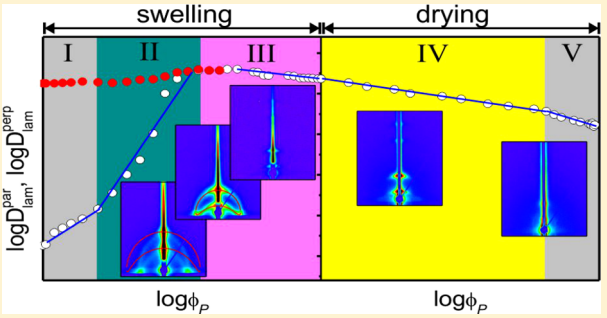

1. INTRODUCTION

Block copolymers self-assemble into a rich variety of periodic patterns, which have a microdomain spacing, D, typically in the range of 10−100 nm. Thin block copolymer films are of increasing importance for many different purposes, such as the preparation of nanoporous films, nanostructured templates, ultrahigh-density data storage media, and biosensors.[1−4] The benefit of these materials depends strongly on the size of the nanostructures, i.e., the microdomain spacing of the copolymer. D can be tuned simply by varying the polymer molar mass because it follows simple scaling laws: $D \propto N^{0.83}$ for $5 < \chi N < 29$ and $D \propto N^{2/3}$ for $\chi N > 29$, where χ is Flory−Huggins segment−segment interaction parameter and N is the degree of polymerization.[1,5] However, defects formed during self-assembly hamper possible applications. Methods to bring the samples into their equilibrium states and to reduce the number of defects are thus highly desirable. To achieve this, solvent vapor annealing (SVA) is an extensively used method.[2−4,6−13] Solvent vapor swells the film and dilutes the polymer, which effectively lowers the glass transition temperatures (T_g) of the polymer blocks, reduces the viscosity, increases chain mobility, and reduces the interfacial tension between the different blocks and between the block copolymer and the substrate.[6] Thus, swelling of both blocks provides sufficient mobility for the chains to rearrange. Moreover, in order to address the challenge of improving the long-range order of the microdomains, it is crucial to understand the structural changes during SVA.

The morphology in the swollen state may play a critical role for the nanostructure after drying. The presence of solvent vapor will change the interfacial tension between the two blocks. As a result, changes of the orientation of the microdomains have been observed in thin films with the cylindrical morphology.[10,14−17] Cavicchi et al. found that, by controlling the film thickness in the fully swollen state and thus

Received: March 27, 2014
Revised: July 29, 2014
Published: August 15, 2014

   dx.doi.org/10.1021/ma500633b | Macromolecules 2014, 47, 5711−5718

the concentration of solvent in the swollen film, films could be obtained which featured either the parallel or the perpendicular cylinder orientations.[14] Gowd et al. investigated the orientational changes of cylindrical thin films using time-resolved in-situ grazing-incidence small-angle X-ray scattering (GISAXS) during annealing with nonselective and selective solvents.[15] In the case of a nonselective solvent, swelling of perpendicular cylinders leads to the parallel orientation, and this reorientation occurs via a disordered state. In contrast, the orientation remains perpendicular in the case of a solvent which is selective for the matrix. This is a consequence of a morphological change from the cylindrical to the body-centered cubic spherical morphology during swelling and further to perpendicular cylinders during drying. Paradiso et al. found in computer simulations that perpendicular cylinders tend to form under modest evaporation rates and relatively weak segregation strengths and relate this behavior to nontrivial, morphology-dependent density correlations present at the ordering front.[18] Thus, characterization of the morphology in the thin film during SVA by time-resolved GISAXS and in-situ measurements of the film thickness, e.g., by white-light interferometry (WLI), are critical in extending our understanding of the SVA.

It is well established that adding a nonselective solvent reduces D by screening the unfavorable interactions between unlike segments at the microdomain interface.[19] The scaling of D with the volume fraction of polymer, ϕ_P, is often approximated by a power law, $D \propto \phi_P^{-\beta}$.[20] It has been found that β depends on the degree of solvent selectivity, the solvent volume fraction, and the morphology of the ordered state. For a nonselective solvent, experiments have shown that β varies from −0.23 to −0.33.[19−23] Self-consistent field calculations of β for the lamellar morphology with nonselective solvents predict a value of $\beta = -0.20$ for the strong segregation limit and $\beta = -0.50$ for the weak segregation limit.[24,25] A recent approach which is based on strong segregation theory but takes into account the finite width of the lamellar interface results in $\beta = -0.17$ for lamellae,[26,27] a value similar to the one predicted previously. For selective solvents, the effect of the addition of solvent on β is more complicated. Experimentally, β has been shown to vary from −0.51 to 0.46 for various systems.[21,22,28] Theoretical works on β for various model copolymer−solvent systems predict that β can vary from −0.31 to 1.00.[25,28] The majority of investigations have focused on the bulk state, and only few studies have addressed the scaling of D in block copolymer thin films in the presence of solvent. In our previous work on a poly(styrene-*b*-butadiene) (P(S-*b*-B)) diblock copolymer thin film, we have found the following dependences in the late stages of the swelling process: (i) In saturated toluene vapor (which is a nonselective solvent) $D_{lam}^{par} \propto \phi_P^{0.35}$, where D_{lam}^{par} is the spacing of lamellae parallel to the substrate;[29] (ii) in saturated cyclohexane (CHX) vapor which is slightly selective for PB, $D_{lam}^{par} \propto \phi_P^{0.27}$;[30] (iii) in nonsaturated CHX vapor, D_{lam}^{par} decreases more weakly when ϕ_P decreases, following $D_{lam}^{par} \propto \phi_P^{0.17}$.[26] The deviation of β for saturated and nonsaturated solvent vapors may be due to the differences of interfacial energies between the constituent blocks and the solvent vapor. The shrinkage of the lamellar spacing during swelling is associated with the mobility of the polymer chains.

The knowledge of the morphology during the SVA process is of fundamental importance to extend our understanding of the SVA method. In the present work, we follow the structural evolution of a lamellar P(S-*b*-B) diblock copolymer thin film during SVA with EAC. From the values of the solubility parameters of PS, PB, and EAC, EAC seems to be a solvent which is slightly selective for the glassy PS which is expected to facilitate structural rearrangements. In our previous studies, we have used toluene and cyclohexane for SVA,[26,29,30] which are—at least when judging from the solubility parameters—less good solvents for PS than EAC and better solvents for PB. By combining in-situ, real-time GISAXS and WLI, both the internal structures and the film thickness are obtained. Mesoscopic and macroscopic information are combined to reveal the mechanism of structural rearrangement. The as-prepared P(S-*b*-B) diblock copolymer thin film shows randomly oriented lamellae. In our previous studies using other solvents, we only focused on the behavior of the parallel lamellae.[29,30] However, herein, the behavior of both the parallel and the perpendicular lamellae in the thin film is investigated, which gives us a clue to fully understand the structural evolution of the thin film during SVA. The equilibrium scaling of the lamellar spacing during swelling and drying is discussed as well.

2. EXPERIMENTAL SECTION

Material. The poly(styrene-*b*-butadiene) (P(S-*b*-B)) diblock copolymer was purchased from Polymer Source Inc., Canada. Its molar mass is 28.0 kg/mol with a PB volume fraction of 0.51 and a dispersity index of 1.05. The overall degree of polymerization, based on the PB monomer volume, is $N = 473$. The Flory−Huggins segment−segment interaction parameter at room temperature, χ, is 0.055;[31] thus, $\chi N = 26$. The critical surface tensions are $\gamma_c = 28$ mN m^{-1} for PB and 33 mN m^{-1} for PS.[32] The solubility parameters of PS and PB are 9.15 and 8.5 (cal cm^{-3})$^{1/2}$, respectively.[33] The mass density of PS is $\rho = 1.05$ g/cm^3, and its glass transition temperature $T_{g,PS} = 76$ °C.[31] Ethyl acetate (EAC) was purchased from Carl Roth GmbH. Its purity is 99.9%. Its solubility parameter is 9.1 (cal cm^{-3})$^{1/2}$,[33] its mass density at room temperature $\rho_{EAC} = 0.897$ g/cm^3, and its $T_{g,EAC} = -154$ °C.[34] Using the Fox equation[35]

$$\frac{1}{T_{g,PS/EAC}} = \frac{\phi\rho_{PS}}{\phi\rho_{PS} + (1-\phi)\rho_{EAC}} \times \frac{1}{T_{g,PS}} + \frac{(1-\phi)\rho_{EAC}}{\phi\rho_{PS} + (1-\phi)\rho_{EAC}} \times \frac{1}{T_{g,EAC}} \quad (1)$$

we estimate that the glass transition of the PS domain during swelling with EAC, $T_{g,PS/EAC}$, reaches room temperature at a polymer volume fraction $\phi = 0.90$. At this, we have assumed that $T_{g,PS}$ is the same as in the bulk and that the solvent is equally distributed in the film.

Sample Preparation. Si(100) wafers (Silchem Handelsgesellschaft mbH) were precleaned for 15 min at 80 °C in an acid bath, followed by rinsing in deionized water and drying with compressed oil-free nitrogen. Then, the cleaned substrates were spin-dried successively with ethanol and acetone, resulting in a hydrophobic surface.[36] The surface energy of the substrate has previously been determined to be 39.5 mN/m.[30] The block copolymer was dissolved in toluene at a concentration of 60 mg mL^{-1} together with ∼2% w/w (relative to the polymer mass) antioxidant (Irganox 1010 from CIBA) to prevent cross-linking of the PB blocks during further treatment. The film was prepared by spin-coating at 3000 rpm for 30 s and was dried at room temperature in vacuum for 24 h. The film thickness was 3260 ± 10 Å. The bulk sample was annealed for 4 h at 120 °C in a vacuum prior to measurement.

Vapor Annealing Protocol. SVA of the film was carried out in a homemade cell (Supporting Information, Figure S1). The details of the cell as well as the vapor treatment protocol have been described by us previously.[37] Swelling of the film was accomplished by letting EAC vapor flow at a rate of ∼0.4 L/h into the sample cell. This was achieved by bubbling N_2 gas through liquid EAC. Swelling was carried out for 40−45 min. Drying of the films was performed by increasing the flow of N_2 gas directly into the cell stepwise from 0 to 3 L/h over 50 min

dx.doi.org/10.1021/ma500633b | Macromolecules 2014, 47, 5711−5718

with time intervals of 5 min while maintaining the flow of EAC vapor. Then, the flow of EAC vapor was stopped, and the direct N_2 gas flow was decreased stepwise to 0 with time intervals of 5 min.

The film thickness was determined by means of WLI (Nanocalc 2000 instrument from Ocean Optics Germany GmbH, Germany) during SVA. The polymer volume fraction during SVA is given by $\phi_P = D_{film}^{dry}/D_{film}$, where D_{film}^{dry} and D_{film} are the film thicknesses of the as-prepared film and the swollen film, respectively. The swelling ratio is defined as $1/\phi_P$. The swelling behavior of PS homopolymer and PB homopolymer is given in Figure S2.

Grazing-Incidence Small-Angle X-ray Scattering (GISAXS). GISAXS experiments were performed at beamline BW4, HASYLAB at DESY in Hamburg, Germany. The wavelength λ was 1.38 Å. At this wavelength, the critical angles of total external reflection of the P(S-*b*-B) film and the SiO_x substrate are $\alpha_{cP} = 0.13°$ and $\alpha_{cS} = 0.20°$, respectively.[38] The incident angle, α_i, was chosen at 0.18°, which is between α_{cP} and α_{cS}; thus, internal film structures could be detected. A MarCCD area detector was used for the detection of the scattered intensity. The pixel size was 79.1 μm × 79.1 μm. The sample−detector distance was 2.52 m, resulting in a q-resolution of 1.43×10^{-4} Å^{-1}/pixel. To protect the detector, the intense reflected beam as well as the intense scattering in the incident plane were attenuated in most cases by a round and a rod-shaped beam stop.

The lamellar orientation was determined from the GISAXS images. Randomly oriented lamellae give rise to rings of high intensity, the so-called diffuse Debye−Scherrer rings (DDSRs).[39,40] The intensity distribution along the rings is indicative of the distribution of lamellar orientations. Using the distorted-wave Born approximation (DWBA),[39−41] the position of the DDSRs is given by

$$q_z = k_{iz} + \sqrt{{k_{cP}}^2 + \left[\sqrt{\left(\frac{2\pi m}{D_{lam}}\right)^2 - {q_y}^2} \pm \sqrt{{k_{iz}}^2 - {k_{cP}}^2}\right]^2} \quad (2)$$

Here, $k_{iz} = k_0 \sin(\alpha_i)$ is the z-component of the wave vector of the incoming beam with $k_0 = 2\pi/\lambda$. k_{cP} is the z-component of wave vector at the critical angle of total external reflection of the polymer film, α_{cP}, $k_{cP} = k_0 \sin(\alpha_{cP})$. D_{lam} is the lamellar spacing, and m is the order of the reflection.

In case of the parallel lamellar orientation, i.e., when the lamellar interfaces are parallel to the substrate, the intensity of the DDSRs in the region of $q_y = 0$ is significantly enhanced, and so-called diffuse Bragg sheets (DBSs) appear along the film normal, q_z. They extend along q_y and are located at regular spacings along the q_z direction. For each value of m, two peaks denoted the "minus branch (M)" and the "plus branch (P)" are expected.

The lamellar spacing of parallel lamellae, D_{lam}^{par}, was deduced from the q_z position of the DBSs. The experimental intensity profiles were compared to profiles calculated using a software based on the DWBA which we have developed previously for the case of diblock copolymer lamellae with weak internal contrast.[40,41] The same model featuring a stack of lamellae consisting of alternating PS and PB layers was used as previously described in detail.[26] In short, the thin film was modeled to consist of D_{film}/D_{lam}^{par} lamellae. The lamellar interfaces were assumed to be perfectly flat and infinitely extended in the film plane. The layer sequence chosen is given in Scheme S1. D_{lam}^{par} and a_i were varied in order to account for small errors in the sample alignment.

If the lamellae are perpendicular to the substrate, the 2D images feature Bragg rods (BRs) which are tangents to the DDSRs and parallel to the q_z axis. The lamellar spacing of perpendicular lamellae, D_{lam}^{perp}, is deduced from the q_y position of the mth order BRs:

$$D_{lam}^{perp} = 2\pi m/q_y \quad (3)$$

To characterize the lateral film structure and to quantify D_{lam}^{perp}, profiles were created along q_y at the q_z value of the center of the specularly reflected beam. D_{lam}^{perp} was obtained by fitting the q_y profiles with a Lorentzian function (see Supporting Information).

For the analysis of the FWHMs, the P1 peak along q_z was chosen for the parallel lamellae because it is the most intense and does not overlap with the specularly reflected beam or the Yoneda region at any time (see Supporting Information, Figure S3a). For the perpendicular lamellae, a Lorentzian function was fitted to the q_y profiles to quantify the FWHM (see Supporting Information, Figure S3b).

Small-Angle X-ray Scattering (SAXS). Transmission SAXS measurements were carried out on the same instrument as the GISAXS measurements. The bulk sample was mounted in a sample holder with a 3 mm diameter opening. The measurement was carried out at room temperature. Thus, the bulk structure of the P(S-*b*-B) diblock copolymer was determined at room temperature by means of SAXS.

3. RESULTS AND DISCUSSION

Knowledge of the structure of the P(S-*b*-B) diblock copolymer in the bulk equilibrium state is mandatory to properly evaluate the thin film results. Thus, the bulk structure of the P(S-*b*-B) diblock copolymer was determined at room temperature by means of SAXS. Figure 1 shows the intensity profile which

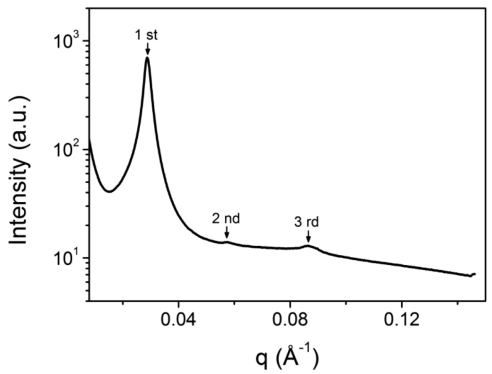

Figure 1. SAXS intensity profile of the bulk sample. The arrows mark the positions of the first-, second-, and third-order Bragg reflections.

features three diffraction peaks. The intensity of the second-order peak is quite weak, compared to the third-order peak, indicating that the lamellae are almost symmetric which is in accordance with the fact that the copolymer is compositionally symmetric. The ratio of the q positions of the three Bragg peaks of 1:1.98:3.01 indicates the presence of a lamellar structure. Using Bragg's law and the peak position of the first-order Bragg reflection, the lamellar spacing is found at $D_{lam}^{bulk} = 220 \pm 4$ Å.

Figure 2a shows selected 2D GISAXS images obtained during SVA. The GISAXS image of the as-prepared film (Figure 2a, image taken at 0 s) shows a pair of first-order DDSRs, their intensities being enhanced between the Yoneda peaks of P(S-*b*-B) and SiO_x, in the so-called Yoneda band.[41] In addition, the intensities of the DDSRs are significantly enhanced near $q_y = 0$; i.e., a significant fraction of the lamellae is parallel to the film surface. Thus, the thin film features mainly parallel lamellae with a small portion of randomly oriented ones.[26,30] We note that this inhomogeneous intensity distribution indicates that the film is not disordered.[30] This is in line with the fact that the χN value of the P(S-*b*-B) diblock copolymer under study is as high as 26, i.e., far higher than the value at the order-to-disorder transition (~10.5). To characterize the inner structure quantitatively, the first-order DDSRs were fitted by eq 2 in the following way: First, to determine the spacing of the parallel lamellae, a q_z profile was created from the experimental 2D GISAXS image by averaging over a narrow q_y range (−0.002 Å^{-1} < q_y < 0.002 Å^{-1}) along q_z (Figure 2b). Second, the lamellar spacing was determined from this q_z profile by using the software and model described in the Experimental Section

dx.doi.org/10.1021/ma500633b | Macromolecules 2014, 47, 5711−5718

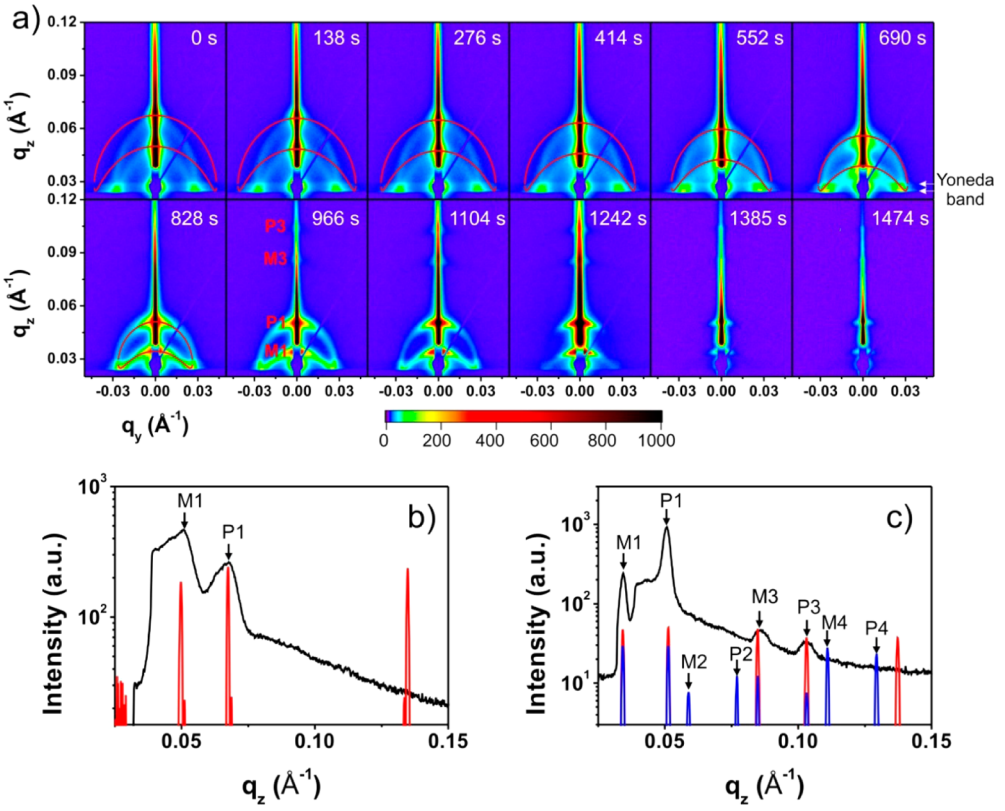

Figure 2. (a) Selected 2D GISAXS images during swelling with EAC vapor. The times after the beginning of the SVA are indicated. The exposure time is 5 s for the images taken at 1385 and 1474 s, else 30 s. The intensity scale is given below the images. The M1, P1, M3, and P3 peaks are marked as well as the Yoneda band; see text. The red arcs are the calculated DDSRs; see text. (b) q_z profile measured at 0 s (black line) and model curve calculated using the symmetric model (red line); see text. (c) q_z profile measured at 966 s (black line) and model curves calculated using the symmetric model (red line) and the asymmetric model (blue line). For the latter, an asymmetry of 0.55 was chosen, just high enough to reveal the position of the M2 and P2 reflections.

and varying the spacing of the parallel lamellae and α_i to match the q_z peak positions of the first-order Bragg reflections M1 and P1. While the calculated curve cannot reproduce the width of the peaks, the peak positions of M1 and P1 are well reproduced (Figure 2b). The best match was obtained for D_{lam}^{par} = 145.5 ± 1 Å and α_i = 0.178 ± 0.001°. The film thickness of 3260 ± 10 Å thus amounts to 22.4D_{lam}^{par}. The value of α_i is very close to the nominal value of 0.18°, which confirms that the sample adjustment is reliable; however, D_{lam}^{par} is significantly smaller than the bulk value. Third, using this D_{lam}^{par} value, the calculated DDSRs were derived from eq 2. It is found that neither the calculated M1 nor the calculated P1 DDSRs fit the measured ones, which indicates that the lamellar spacing depends on the orientation of the lamellae, whereas the parallel lamellar spacing is much smaller than the perpendicular. Using Bragg's law, we find D_{lam}^{perp} = 230 ± 1 Å, which is close to the value of bulk sample. Shear forces during the film preparation by spin-coating may be at the origin of the orientation dependence of the lamellar spacing. We anticipate that such kind of inner structure may give rise to different behaviors for parallel and perpendicular lamellae during SVA.

During swelling, the lamellae start to rearrange: After 966 s (D_{film} = 3970 Å), higher order DBSs (marked M3 and P3) appear as a consequence of the appearance of long-range order of the parallel lamellae (Figure 2a). Figure 2c shows the corresponding q_z profile together with a fit to the same model as in the dry state, i.e., symmetric lamellae with D_{lam}^{perp} = 239 ± 0.5 Å and α_i = 0.178 ± 0.001° (red line). It demonstrates that the higher-order DDSRs are the third-order M3 and P3 reflections. Increasing the asymmetry of the lamellae, e.g., by using a volume fraction of PB of 0.55 (asymmetric model), results in the same M1, P1, M3, and P3 reflections and in additional even-order peaks, M2, P2, M4, and P4. (This asymmetry was chosen to be just high enough to reveal the *positions* of the even-order peaks.) The M2 and P2 peaks are not present in the experimental q_z profile; i.e., the lamellae are still symmetric in the swollen state. Thus, EAC acts as a nonselective solvent for P(S-*b*-B), which is consistent with the results got from swelling homopolymers (Figure S2). At the end of the swelling (Figure 2a, 1474 s, D_{film} = 4201 Å), the DDSRs have vanished, and the GISAXS images only show DBSs, indicating that the perpendicular lamellae disappear at the end of the swelling process, and a thin film with completely parallel lamellae is obtained. At this stage, the exposure time had to be reduced from 30 to 5 s because the intensity of the DBSs was very high (see images at 1385 and 1474 s in Figure 2a). This is counterintuitive because EAC is shown to be distributed evenly among the two blocks, which is expected to reduce the contrast between the swollen PS and PB domains resulting in weaker DBSs. Thus, the increase of the DBSs' intensity indicates that well-correlated and long-range ordered parallel lamellae are formed during the swelling process. We speculate that the reorientation of the lamellae from the random orientation to a completely parallel orientation starts by the formation of parallel lamellae at the top surface, since there the polymer mobility is highest. This is in accordance

dx.doi.org/10.1021/ma500633b | *Macromolecules* 2014, 47, 5711−5718

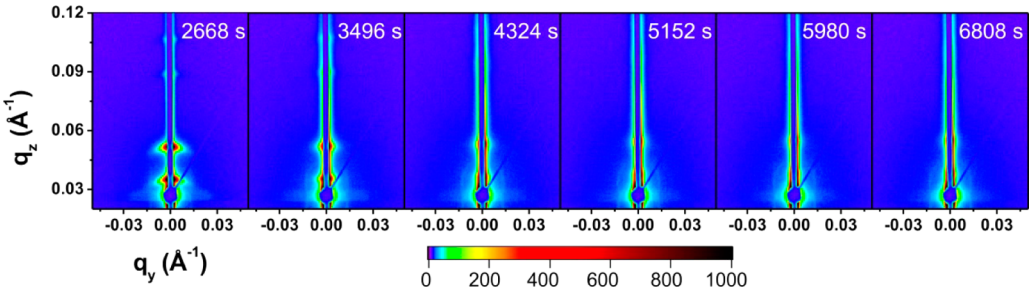

Figure 3. Selected 2D GISAXS images during drying. The times after the beginning of the SVA are indicated. The exposure time is 30 s for all images. The intensity scale is given at the bottom.

with theoretical work on the structure formation in block copolymer thin films.[17,18,42] Since the PB block has the lower surface energy of the two blocks, the such formed parallel lamellae are stable during swelling. Thus, reorientation involves the propagation of changes at the free surface through the film toward the substrate as a front.[11,42]

The behavior of the lamellar spacing for different orientations is characterized by comparing the measured DDSRs with the ones calculated using D_{lam}^{par}. It is clearly seen that the fits match the shape of the measured DDSRs better and better in the course of the swelling until complete agreement is reached at 828 s and onward. This means a homogeneous lamellar spacing is obtained regardless of the lamellar orientation. The swelling behavior of the parallel and perpendicular lamellae is thus different since their lamellar spacing is vastly different in the as-prepared thin film but becomes equal during swelling with solvent vapor.

Qualitatively, the structural rearrangements during swelling can be divided into two steps: (i) initially, the swelling behavior of the lamellae depends on their orientation until a homogeneous lamellar spacing is reached; (ii) later, the orientational distribution of the lamellae changes and a completely parallel orientation is obtained at the end of the swelling process. A quantitative analysis is given below.

We now turn to the drying process. Figure 3 shows selected 2D GISAXS images during drying. Owing to the intense DBSs and the intense diffuse scattering in the plane of incidence, a rod-shaped beam stop had to be used to protect the detector. Only the first- and third-order DBSs are present, and no DDSRs appear, indicating that only the parallel lamellae persist during and after drying and that they are symmetric. Such behavior is to be expected because (i) it costs energy and requires a large-scale mass transport to form tilted lamellae out of parallel lamellae, therefore this is hindered, and (ii) the polymers lose mobility as the solvent evaporates gradually during drying which additionally hampers reorientation.

To quantitatively analyze the data, q_z profiles and q_y profiles were created following the previously described procedure, from the experimental 2D GISAXS images. The lamellar spacings were obtained using the model described in the Experimental Section for the parallel lamellae and Bragg's law for the perpendicular lamellae, respectively. Figure 4a shows the reduced lamellar spacings (normalized to the bulk value of D_{lam}^{bulk} = 220 Å) and the reduced film thickness (normalized to the value of the as-prepared film, 3260 Å) as a function of time during SVA. For the as-prepared thin film, it is clearly seen that the perpendicular lamellae (red solid circles in Figure 4a) have the same spacing as the bulk sample, namely $D_{lam}^{perp} = 1.02D_{lam}^{bulk}$, whereas the spacing of the parallel lamellae (black open circles

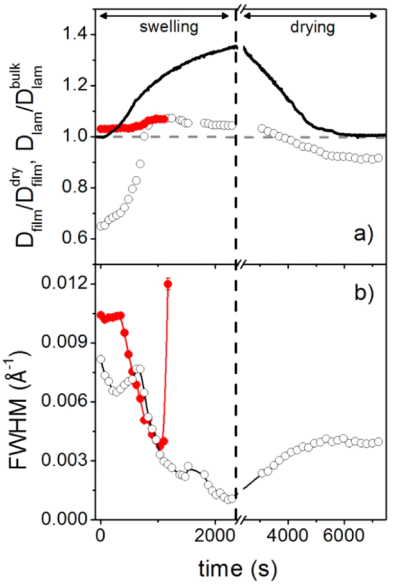

Figure 4. (a) Reduced film thickness (black line) and reduced lamellar spacings (parallel lamellae: black open circles; perpendicular lamellae: red solid circles) during solvent vapor annealing. The horizontal dashed line indicates the value of one. (b) FWHMs of the DBSs along q_z (parallel lamellae, black open circles) and the DBSs along q_y (perpendicular lamellae, red solid circles). The vertical dashed line marks the beginning of the drying process.

in Figure 4a), is only $D_{lam}^{par} = 0.65D_{lam}^{bulk}$, i.e., much lower than D_{lam}^{bulk}.

During swelling, the film thickness increases within 2410 s gradually to $1.35D_{film}^{dry}$ (Figure 4a). D_{lam}^{perp} initially stays constant and then increases slightly to $1.07D_{lam}^{bulk}$. A major change of D_{lam}^{perp} is not observed because it already matches the equilibrium value. In contrast, D_{lam}^{par} increases very rapidly from $0.65D_{lam}^{bulk}$ to $1.07D_{lam}^{bulk}$, where it reaches the value of D_{lam}^{perp} after approximately 828 s. At this time, the glass transition temperature of the PS domains reaches room temperature (see below). Soon after, the perpendicular lamellae disappear (see Figure 2a). For the remaining time of the swelling process, D_{lam}^{par} decreases.

During drying, both D_{film} and D_{lam}^{par} decrease, however, with different tendencies. D_{film} decreases at a rate of −25 Å/min and reaches the same value as in the as-prepared film; i.e., no more solvent is present in the film. The final value of D_{lam}^{par} is $0.91D_{lam}^{bulk}$, which is larger than in the as-prepared film ($0.65D_{lam}^{bulk}$) and very close to the bulk value.

To characterize the lamellar correlation, the FWHMs of the P1 peak of the DBSs along q_z (due to the parallel lamellae, black open circles) and the Bragg rods along q_y (due to the perpendicular lamellae, red solid circles) were determined by

dx.doi.org/10.1021/ma500633b | Macromolecules 2014, 47, 5711−5718

fitting a Gaussian function (Figure S3a) or a Lorentzian function (Figure S3b) to the intensity profiles, respectively. The results are shown in Figure 4b. It is striking that the behavior of the parallel lamellae is more complex than the one of the perpendicular lamellae. For the perpendicular lamellae, first, the FWHM decreases and reaches a minimum at 1040 s, which indicates that the correlation of the perpendicular lamellae improves during swelling. Second, the FWHM increases rapidly; i.e., the stack size decreases strongly until the perpendicular lamellae vanish completely (see the 2D images in Figure 2a). For the parallel lamellae, a maximum is encountered after 600 s of swelling (Figure 4b) which means a partial loss of correlation, which may be ascribed to a breakup and reorganization of the lamellar stack. The subsequent decrease of the FWHM until 1350 s means that well-correlated, parallel lamellae are formed, which is consistent with the above-described strong increase of the intensity of the DBSs. However, when D_{lam}^{par} starts to decrease after 1350 s (Figure 4a), the FWHM features another maximum at 1500 s (Figure 4b), which proves that another breakup and reorganization of the lamellar stack takes place which is necessary to form thinner lamellae. During drying, the FWHM slightly increases, which means the ordering of the lamellae becomes worse. We attribute this to the fact that the lamellae rearranged as a result of the increased effective Flory–Huggins interaction between different blocks as the solvent was removed from the thin film. We hypothesize that the fully swollen lamellae near the film surface dry first and change their lamellar thickness. The depletion of solvent proceeds downward, i.e. toward the substrate surface, but it becomes increasingly difficult for the solvent to diffuse through the relatively dry top layer. At the same time, the mobility of P(S-*b*-B) decreases, especially when the glass transition of PS is crossed. This way, defects may freeze in, and the final degree of order is slightly worse than in the fully swollen state.

To quantify the dependence of the lamellar spacing, D_{lam}, on the polymer volume fraction, ϕ_P, $D_{lam} \propto \phi_P^{-\beta}$, we have plotted D_{lam}^{par} and D_{lam}^{perp} during SVA as a function of ϕ_P in a log–log representation (Figure 5). For the behavior of the parallel lamellae, three regimes are identified: (I) slow swelling following $D_{lam}^{par} \propto \phi_P^{-2.2\pm0.3}$ for $0.95 < \phi_P < 1$, (II) faster swelling following $D_{lam}^{par} \propto \phi_P^{-5.1\pm0.3}$ for $0.87 < \phi_P < 0.95$, and (III) a slow deswelling following $D_{lam}^{par} \propto \phi_P^{0.32\pm0.3}$ for $0.77 < \phi_P < 0.83$. These regimes are indicated in Figure 5 by different colors, and the corresponding times are given in the top axis.

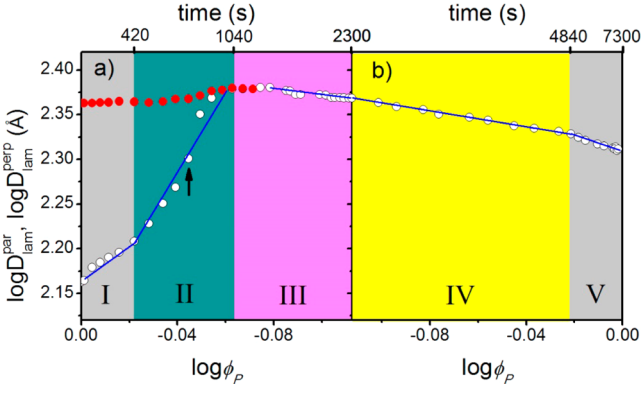

Figure 5. Lamellar spacings, D_{lam}^{par} (open black circles) and D_{lam}^{perp} (red solid circles), as a function of the polymer volume fraction, ϕ_P, in a double-logarithmic representation during swelling (a) and drying (b). The full lines are linear fits. The background colors indicate the different regimes marked by Roman numbers. The corresponding times are given on the top axis of the profiles. The arrow indicates the polymer concentration at which the glass transition temperature of PS block reaches room temperature.

The initial swelling (I) is faster than expected from simple volume addition, i.e., the affine swelling predicted by mean field theory, $D_{lam} \propto \phi_P^{-1}$, where it is assumed that the interfacial area per chain is unchanged from the dry state.[43] We propose that the observed behavior is due to inhomogeneous swelling. It may be due to an interface effect because the penetration of the solvent into the film proceeds mainly through the interfaces.[27] In this way, the solvent shields unfavorable contacts between PS and PB, thus decreasing the enthalpic contribution to the total free energy. Our previous studies have shown that the distribution of lamellar orientations is inhomogeneous: Parallel lamellae are mainly present near the film surface, whereas perpendicular lamellae prevail near the film–substrate interface.[26] Thus, the uppermost parallel lamellae swell first when the solvent vapor treatment is started, which is reflected by the movement of the DBSs. In contrast, ϕ_P is calculated by the variation of D_{film}, i.e., the solvent content averaged over the entire film which may be lower than the one in the parallel lamellae near the film surface. Together, these effects result in the behavior $D_{lam}^{par} \propto \phi_P^{-2.2\pm0.3}$.

The change of exponent β to a significantly higher value (regime II) is due to the fact that the glass transition of PS is crossed by taking up solvent.[44] The arrow indicates the polymer concentration at which the glass transition temperature of PS block at room temperature, calculated by eq 1, takes place. The concentration of the polymer is lower than the beginning of regime II which is due to the inhomogeneous swelling as discussed above. D_{lam}^{par} in the as-prepared thin film is much lower than D_{lam}^{bulk}; i.e., it is far away from the equilibrium state. Solvent uptake leads to an increase in polymer mobility, which facilitates these structural rearrangements. Thus, thicker lamellae are formed. This significant rearrangement is indeed reflected by a maximum of the FWHM in the corresponding regime (Figure 4b, 600 s, ϕ_P =0.9). Thus, the thickening of the parallel lamellae leads to a high value of β. At the end of regime II, D_{lam}^{par} and D_{lam}^{perp} are equal. This time coincides with the point where T_g of PS has reached room temperature.

The subsequent weak decrease of D_{lam}^{par} (regime III) has been observed by us previously and has been attributed to the formation of additional lamellae.[26,27,29,30] These are formed to accommodate the swollen and coiled block copolymers, which results in a decrease of D_{lam}^{par}. The rearrangement of the lamellae is reflected by the second maximum of the FWHM of the DBSs in this regime (Figure 4b, 1500 s, ϕ_P =0.81). In the present study, $\beta = -0.32$ is found which is very similar to the value $\beta = -0.35$ which was obtained by us previously during toluene vapor annealing (nonselective solvent).[29] It is in agreement with the theoretical prediction as well.[43] However, it is different from the value $\beta = -0.17$ which was obtained during CHX vapor treatment (slightly selective solvent for PB).[26] As discussed above, the present GISAXS result shows that EAC is a nonselective solvent for both blocks because no even order peaks appear during swelling. Moreover, it has been demonstrated that variations in solvent selectivity can lead to a substantial variation in β.[22]

During drying, two regimes are distinguished (Figure 5b): (IV) slow deswelling following $D_{lam}^{par} \propto \phi_P^{-0.43\pm0.01}$ for $0.77 < \phi_P < 0.95$ and (V) faster deswelling following $D_{lam}^{par} \propto \phi_P^{-0.84\pm0.04}$

dx.doi.org/10.1021/ma500633b | Macromolecules 2014, 47, 5711–5718

for $0.95 < \phi_P < 1$. The initial drying (IV) is slower than expected for affine deswelling; i.e., the lamellar spacing is higher than that resulting from affine deswelling. As the solvent is removed, nonfavorable segmental interactions increase, and the block copolymers undergo a reorganization within the entire film to accommodate the incommensurability between the surface area and the changing lamellar spacing. This means that additional thicker lamellae are formed via rearrangement of the lamellae, which is possible because, at this degree of swelling, the T_g of the PS domains is still below room temperature.[44] The behavior is different from the one which shows an increase of domain spacing during the deswelling process observed by Gu et al.[9] However, in both cases the lamellar thickness tends to reach the bulk equilibrium value. The subsequent drying (V) is affine. The beginning of this regime is at the same ϕ_P (Figure 4, $\phi_P = 0.95$) as the beginning of the second regime of swelling; i.e., in this regime, T_g of PS is now above room temperature, which drastically reduces the mobility of the PS blocks and leads to a different drying mechanism. Owing to the low T_g of PB, further evaporation of the solvent is expected to give rise to asymmetric lamellae. This speculation is supported by the experimental data. Figure 6 shows the q_z profiles at the beginning and at the end of the second drying regime (V). The second-order DBSs M2 and P2 appear after drying, indicating that asymmetric lamellae are formed.

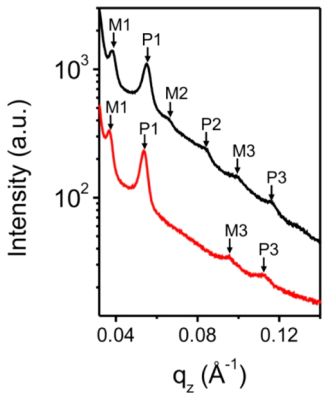

Figure 6. q_z profiles at the beginning (4800 s, $\phi_P = 0.95$, lower red curve) and at the end (7200 s, $\phi_P = 1.0$, upper black curve) of the second regime of drying (V). The curves are shifted vertically for better visibility. M1, P1, M2, P2, M3, and P3 mark the DBSs.

4. CONCLUSION

In summary, we have investigated the structural evolution of a poly(styrene-*b*-butadiene) diblock copolymer thin film having initially a distribution of lamellar orientations during annealing with EAC vapor. The behavior of both the parallel and the perpendicular lamellae in the thin film is investigated in detail, which gives us a clue to fully understand the reorganizational processes during SVA. The structural evolution of the thin film can be described by the sketch shown in Figure 7. For the as-prepared sample, the lamellar spacing depends on the orientation of the lamellae. Whereas the parallel lamellae have the smallest spacing, the perpendicular ones have the largest one (Figure 7a). During swelling, the perpendicular lamellae swell less easily than the parallel ones because of the constraining effect of the substrate. However, both reach the same lamellar spacing after a certain time of swelling (Figure 7b). The orientational distribution of the lamellae is changed during swelling, and a completely parallel orientation is obtained at the end of the swelling process (Figure 7c). For $0.87 < \phi_P < 0.95$, the lamellar spacing increases and reaches the bulk (equilibrium) value. Unexpectedly, EAC turns out to act as a nonselective solvent for P(S-*b*-B) diblock copolymer. It screens the unfavorable interactions between the PS and PB blocks, resulting in a decrease in the lamellar spacing with increasing solvent concentration. For $0.77 < \phi_P < 0.83$, we find a scaling exponent, $\beta = -0.32$, which is in agreement with the theoretical prediction.[43] Comparing with previous results on a thin film featuring initially parallel lamellae and being swollen in toluene,[29] we find that the increase of D_{lam}^{par} is different, whereas the subsequent decrease during the later stage of the swelling follows the same behavior. After drying, a thin film with exclusively parallel lamellae is obtained; however, their spacing, $0.91D_{lam}^{bulk}$, is larger than in the as-prepared film, $0.65D_{lam}^{bulk}$ (Figure 7d).

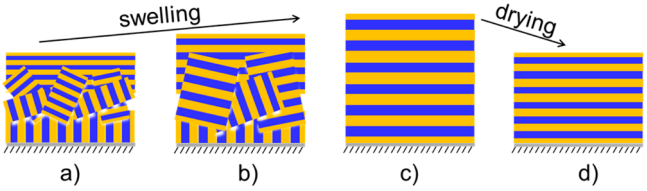

Figure 7. Schematic structures of the thin film during swelling and drying: (a) as-prepared film at $t = 0$ s, (b) swollen film at $t = 828$ s, (c) swollen film at $t = 1350$ s, (d) subsequently dried film at $t = 7200$ s.

In this study, the swelling related morphology evolution is studied by GISAXS combined with WLI. The knowledge of the reorganizational processes during SVA—as the thin film swells, deswells, and goes through thickness and intermediate morphology changes—is of fundamental importance to understand the origin of the final film morphology after drying.

■ ASSOCIATED CONTENT

Ⓢ Supporting Information

Schematic drawing of the model used for calculating the intensity profiles; sketch of our homemade SVA setup; FWHM of the scattering profiles. This material is available free of charge via the Internet at http://pubs.acs.org.

■ AUTHOR INFORMATION

Corresponding Author

*E-mail: zhangjq@nanoctr.cn (J.Z.).

Present Addresses

J.Z.: National Center for Nanoscience and Technology, Beijing 100190, P. R. China.

S.J.: Forschungszentrum Jülich GmbH, JCNS at Heinz Maier-Leibnitz Zentrum, Lichtenbergstr. 1, D-85747 Garching, Germany.

Notes

The authors declare no competing financial interest.

■ ACKNOWLEDGMENTS

We thank I. I. Potemkin for fruitful discussions, A. Sepe for developing the SVA cell and F. Jung for carrying out SVA experiments on homopolymers. We acknowledge funding by DFG (Pa771/7-1). We thank Deutsches Elektronen-Synchrotron for beamtime and excellent equipment. D.P. thanks DANSCATT (Danish Centre for the Use of Synchrotron X-ray and Neutron Facilities) for financial support. CHESS is

supported by NSF & NIH/NIGMS via NSF award DMR-1332208.

REFERENCES

(1) Hamley, I. W. *The Physics of Block Copolymers*; Oxford University Press: New York, 1998.
(2) Fukunaga, K.; Elbs, H.; Magerle, R.; Krausch, G. *Macromolecules* **2000**, *33*, 947−953.
(3) Tada, Y.; Yoshida, H.; Ishida, Y.; Hirai, T.; Bosworth, J. K.; Dobisz, E.; Ruiz, R.; Takenaka, M.; Hayakawa, T.; Hasegawa, H. *Macromolecules* **2012**, *45*, 292−304.
(4) Gotrik, K. W.; Hannon, A. F.; Son, J. G.; Keller, B.; Alexander-Katz, A.; Ross, C. A. *ACS Nano* **2012**, *6*, 8052−8059.
(5) Papadakis, C. M.; Almdal, K.; Mortensen, K.; Posselt, D. *Europhys. Lett.* **1996**, *36*, 289−294.
(6) Sinturel, C.; Vayer, M.; Morris, M.; Hillmyer, M. A. *Macromolecules* **2013**, *46*, 5399−5415.
(7) Gotrik, K. W.; Ross, C. A. *Nano Lett.* **2013**, *13*, 5117−5122.
(8) Kim, E.; Ahn, H.; Park, S.; Lee, H.; Lee, M.; Lee, S.; Kim, T.; Kwak, E.-A.; Lee, J. H.; Lei, X.; Huh, J.; Bang, J.; Lee, B.; Ryu, D. Y. *ACS Nano* **2013**, *7*, 1952−1960.
(9) Gu, X.; Gunkel, I.; Hexemer, A.; Gu, W.; Russell, P. T. *Adv. Mater.* **2014**, *26*, 273−281.
(10) Paik, M. Y.; Bosworth, J. K.; Smilges, D.-M.; Schwartz, E. L.; Andre, X.; Ober, C. K. *Macromolecules* **2010**, *43*, 4253−4260.
(11) Kim, S. H.; Misner, M. J.; Xu, T.; Kimura, M.; Russell, T. P. *Adv. Mater.* **2004**, *16*, 226−231.
(12) Kim, S. H.; Misner, M. J.; Yang, L.; Gang, O.; Ocko, B. M.; Russell, T. P. *Macromolecules* **2006**, *39*, 8473−8479.
(13) Cavicchi, K. A.; Berthiaume, K. J.; Russell, T. P. *Polymer* **2005**, *46*, 11635−11639.
(14) Cavicchi, K. A.; Russell, T. P. *Macromolecules* **2007**, *40*, 1181−1186.
(15) Gowd, E. B.; Böhme, M.; Stamm, M. *IOP Conf. Ser.: Mater. Sci. Eng.* **2010**, *14*, 012015.
(16) Mokarian-Tabari, P.; Collins, T. W.; Holmes, J. D.; Morris, M. A. *ACS Nano* **2011**, *5*, 4617−4623.
(17) Phillip, W. A.; Hillmyer, M. A.; Cussler, E. L. *Macromolecules* **2010**, *43*, 7763−7770.
(18) Paradiso, S. P.; Delaney, K. T.; Garcia-Cervera, C. J.; Ceniceros, H. D.; Fredrickson, G. H. *ACS Macro Lett.* **2014**, *3*, 16−20.
(19) Shibayama, M.; Hashimoto, T.; Hasegawa, H.; Kawai, H. *Macromolecules* **1983**, *16*, 1427−1433.
(20) Shibayama, M.; Hashimoto, T.; Kawai, H. *Macromolecules* **1983**, *16*, 16−28.
(21) Hanley, K. J.; Lodge, T. P. *J. Polym. Sci., Part B: Polym. Phys.* **1998**, *36*, 3101−3113.
(22) Lai, C. J.; Russel, W. B.; Register, R. A. *Macromolecules* **2002**, *35*, 4044−4049.
(23) Lodge, T. P.; Hanley, K. J.; Pudil, B.; Alahapperuma, V. *Macromolecules* **2003**, *36*, 816−822.
(24) Whitmore, M. D.; Noolandi, J. *J. Chem. Phys.* **1990**, *93*, 2946−2955.
(25) Vavasour, J. D.; Whitmore, M. D. *Macromolecules* **2001**, *34*, 3471−3483.
(26) Di, Z.; Posselt, D.; Smilgies, D.-M.; Li, R.; Rauscher, M.; Potemkin, I. I.; Papadakis, C. M. *Macromolecules* **2012**, *45*, 5185−5195.
(27) Rudov, A. A.; Patyukova, E. S.; Neratova, I. V.; Khalatur, P. G.; Posselt, D.; Papadakis, C. M.; Potemkin, I. I. *Macromolecules* **2013**, *46*, 5786−5795.
(28) Hanley, K. J.; Lodge, T. P.; Huang, C. I. *Macromolecules* **2000**, *33*, 5918−5931.
(29) Papadakis, C. M.; Di, Z.; Posselt, D.; Smilgies, D.-M. *Langmuir* **2008**, *24*, 13815−13818.
(30) Di, Z.; Posselt, D.; Smilgies, D.-M.; Papadakis, C. M. *Macromolecules* **2010**, *43*, 418−427.
(31) Papadakis, C. M.; Almdal, K.; Mortensen, K.; Posselt, D. *J. Phys. II* **1997**, *7*, 1829−1854.
(32) Turturro, A.; Gattiglia, E.; Vacca, P.; Viola, G. T. *Polymer* **1995**, *36*, 3987−3996.
(33) Rudd, J. F. *Polymer Handbook*, 2nd ed.; Brandrup, J., Immergut, E. H., Eds.; Wiley: New York, 1989.
(34) Ellis, T. S.; Karasz, F. E.; Tenbrinke, G. *J. Appl. Polym. Sci.* **1983**, *28*, 23−32.
(35) Fox, T. G.; Loshaek, S. *J. Polym. Sci.* **1955**, *15*, 371−390.
(36) Müller-Buschbaum, P. *Eur. Phys. J. E* **2003**, *12*, 443−448.
(37) Zhang, J.; Posselt, D.; Sepe, A.; Shen, X.; Perlich, J.; Smilgies, D.-M.; Papadakis, C. M. *Macromol. Rapid Commun.* **2013**, *34*, 1289−1295.
(38) Tolan, M. *X-Ray Scattering from Soft-Matter Thin Films. Materials Science and Basic Research*; Springer-Verlag: Berlin, 1999.
(39) Busch, P.; Posselt, D.; Smilgies, D. M.; Rauscher, M.; Papadakis, C. M. *Macromolecules* **2007**, *40*, 630−640.
(40) Busch, P.; Rauscher, M.; Moulin, J.-F.; Müller-Buschbaum, P. *J. Appl. Crystallogr.* **2011**, *44*, 370−379.
(41) Busch, P.; Rauscher, M.; Smilgies, D. M.; Posselt, D.; Papadakis, C. M. *J. Appl. Crystallogr.* **2006**, *39*, 433−442.
(42) Albert, J. N. L.; Young, W.-S.; Lewis, R. L., III; Bogart, T. D.; Smith, J. R.; Epps, T. H., III. *ACS Nano* **2012**, *6*, 459−466.
(43) Noolandi, J.; Hong, K. M. *Ferroelectrics* **1980**, *30*, 117−123.
(44) Bercea, M.; Wolf, B. A. *J. Chem. Phys.* **2006**, *124*, 174902.